

Article

Enhanced Friction and Wear Properties of TiN/MoS₂ Composite Coating on the Surface of Plasma Nitrided Ti6Al4V Alloy

Hongyu Li ^{1,2}, Kai Le ^{3,4}, Ganggang Wang ², Zhenghao Ren ² , Yuzhen Liu ³, Zhenglong Yang ^{1,*}, Liwei Zheng ^{2,*} and Shusheng Xu ^{3,4} 

¹ School of Chemistry and Materials Science, Ludong University, Yantai 264025, China

² Shandong Laboratory of Advanced Materials and Green Manufacturing at Yantai, Yantai 264000, China; renzhenghao@amgm.ac.cn (Z.R.)

³ State Key Laboratory of Solid Lubrication, Lanzhou Institute of Chemical Physics, Chinese Academy of Sciences, Lanzhou 730000, China; sxxu@licp.cas.cn (S.X.)

⁴ Yantai Zhongke Research Institute of Advanced Materials and Green Chemical Engineering, Yantai 264000, China

* Correspondence: yzl@iccas.ac.cn (Z.Y.); liweizheng@amgm.ac.cn (L.Z.); Tel.: +86-535-6010206 (L.Z.)

Abstract: In this study, plasma nitriding and multi-arc ion plating techniques were employed to enhance the load-bearing capacity of the TC4 alloy. The tribological properties were characterized, and the mechanisms were discussed in detail. Subsequently, the tribological properties of the coating enhanced with MoS₂ were then evaluated, and the results indicated that the plasma nitriding treatment, which exhibited optimal friction performance, resulted in the formation of a nitrided layer with a thickness of 98 μm on the surface of the TC4 alloy, thereby significantly improving its mechanical properties. Furthermore, the TiN coating samples treated with plasma nitriding demonstrated superior mechanical properties, achieving the highest hardness value (20 GPa), high load-carrying capacity (58 N) and the lowest wear rate ($9.16 \times 10^{-6} \text{ mm}^3 \cdot \text{N}^{-1} \cdot \text{m}^{-1}$). Moreover, the tribological properties of MoS₂ deposited on the surface of the PN-2/TiN sample were significantly enhanced, which can be attributed to the synergistic effect of the excellent load-bearing characteristics of the plasma nitriding treatment and the wear resistance of the TiN layer. This study investigates the factors contributing to the superior tribological performance of the PN-2/TiN sample and the extended friction lifetime of the PN-2/TiN/MoS₂ sample. The composite coating provides a new method to improve the anti-friction of soft metals, especially titanium alloys, and is expected to be applied in the aerospace field.

Keywords: TC4 alloy; plasma nitriding; TiN coating; MoS₂ coating; bearing capacity; tribology



Received: 20 December 2024

Revised: 13 January 2025

Accepted: 15 January 2025

Published: 16 January 2025

Citation: Li, H.; Le, K.; Wang, G.; Ren, Z.; Liu, Y.; Yang, Z.; Zheng, L.; Xu, S. Enhanced Friction and Wear Properties of TiN/MoS₂ Composite Coating on the Surface of Plasma Nitrided Ti6Al4V Alloy. *Lubricants* **2025**, *13*, 37. <https://doi.org/10.3390/lubricants13010037>

Copyright: © 2025 by the authors. Licensee MDPI, Basel, Switzerland. This article is an open access article distributed under the terms and conditions of the Creative Commons Attribution (CC BY) license (<https://creativecommons.org/licenses/by/4.0/>).

1. Introduction

Ti6Al4V (TC4) alloy is characterized by exceptional tensile strength and resilience, exhibiting outstanding mechanical properties even at extreme temperatures. With its low density, high specific strength, excellent thermal stability, and notable biocompatibility and corrosion resistance, TC4 alloy is a highly versatile material [1,2]. These advantages have established TC4 alloy as a key material in critical applications, including aircraft engines and gas turbine components, as well as in rockets, missiles, and structural components of high-speed aircraft [3–6]. However, the TC4 alloy exhibits limitations such as relatively low strength, elastic modulus, yield strength, and resistance to plastic deformation, which pose challenges for its broader adoption in aerospace and other

high-performance industries [7–9]. To address these limitations, surface engineering technologies have emerged as an effective strategy to enhance the surface properties of TC4 alloy while preserving its inherent advantages.

Applying hard coatings to the surface of the TC4 alloy effectively enhances its load-bearing capacity and wear resistance. This enhancement results from the formation of a robust surface layer with increased strength and hardness. Numerous surface protection methods such as plasma spraying [10], laser shock peening (LSP) [11], micro-arc oxidation (MAO) [12], physical vapor deposition (PVD) [13], chemical vapor deposition (CVD) [14], and thermal oxidation [15] have been developed to enhance the surface mechanical and tribological properties of TC4 alloys. Among these methods, PVD technology has attracted attention owing to its advantageous features. The coatings prepared by PVD exhibit superior hardness, excellent wear resistance, and the ability to deliver consistent performance under demanding conditions [16]. PVD is widely used in industrial manufacturing due to its efficient and versatile deposition process, which produces coatings with excellent adhesion and uniformity. These advantages make PVD one of the most effective methods for developing hard coatings on alloy surfaces. However, the distinct material characteristics of TC4 titanium alloy, compared to conventional steel, make a uniform hardening process insufficient for improving its mechanical properties. Achieving mechanical compatibility in titanium alloys requires implementing gradient mechanical properties, which can be realized using glow ion nitriding technology [17].

Ion nitriding generates a gradient nitrogen concentration within the nitrided layer through diffusion from the surface to the interior. This gradient structure reduces the stress differential between the internal and surface regions, strengthens interfacial bonding between the hardened layer and the substrate, and enhances wear and crack resistance. Additionally, a hardened composite layer is applied on the nitrided layer using PVD technology, significantly enhancing bonding properties [18]. Previous studies have shown that ion nitriding layers and titanium nitride (TiN) coatings greatly enhance wear resistance but exhibit a high coefficient of friction, resulting in significant wear damage and increased energy consumption [19]. To address this challenge, the application of lubricants to the surface is essential. Solid lubricants provide a cost-effective solution to reduce friction and wear. Molybdenum disulfide (MoS₂) is particularly notable among solid lubricants for its excellent properties, which are primarily attributed to its layered structure. Within a single layer, Mo-S bonds exhibit strong covalent interactions, whereas adjacent layers interact via weaker van der Waals forces [20]. This structure allows relative slip between layers. The weak interlayer forces in MoS₂ promote relative slip, enabling effective lubrication [21]. Furthermore, compared to other solid lubricants, the MoS₂ coating demonstrates superior properties, including a low friction coefficient in vacuum or dry environments and a high load-carrying capacity, making it an ideal choice for solid lubrication applications [22,23].

This study employed three distinct treatment processes designed to address the inadequacies in surface load-bearing capacity and the reduction in friction associated with the TC4 alloy, with the objective of enhancing overall tribological performance. First, the TC4 substrate was plasma nitrided. Next, a TiN coating was applied using PVD technology. Finally, a MoS₂ lubrication layer was deposited on the hardened surface via the alcohol droplet method. The mechanical properties of the treated TC4 substrate were investigated, and the tribological performance of the MoS₂ coating applied to various samples was analyzed. The results indicate that plasma nitriding and PVD substantially improve the surface hardness and elastic modulus of the TC4 substrate. Additionally, the wear rate of the PN-2/TiN sample under dry friction conditions was significantly reduced. The enhanced hardness also provides optimal support for the surface MoS₂ coating, thereby improving the overall tribological properties of the workpiece. Previous studies on the

tribology of TC4 alloy have primarily focused on either strengthening and toughening or surface lubrication, with minimal attention given to the integration of both aspects. This limited focus has limited the range of practical applications. In contrast, this study combines both toughness and lubrication, and a novel approach for collaborative protection and lifespan extension is proposed, providing titanium alloys with an effective combination of surface toughness, wear resistance, low friction, and environmental adaptability.

2. Materials and Methods

2.1. Pre-Treatments of TC4 Substrate and Coating Preparation

The thickness of the TC4 substrate is 5 mm and its diameter is 25 mm. Prior to machining, the substrates were polished using progressively finer grit sandpaper, ranging from 400 to 2000. After polishing, the samples were subjected to ultrasonic cleaning, which involved immersing them in acetone and anhydrous ethanol for 10 min each. The sample preparation process consisted of three distinct stages. The TC4 substrates were first positioned in a specialized nitriding furnace for the plasma nitriding process. The procedure was conducted at a temperature of 800 °C for a duration of four hours, under a vacuum pressure of less than 20 Pa, employing a nitrogen–hydrogen gas mixture in a ratio of 3:1. Initially, plasma radiofrequency power of 50 W was applied at 800 °C for 4 h. Subsequently, three treatments were performed using plasma radiofrequency powers of 50, 150, and 300 W, each lasting 30 min, categorized as PN-1, PN-2, and PN-3, respectively. TiN coating deposition was achieved using multi-arc ion plating (MIP). The chamber was first heated to 400 °C, then evacuated to a low pressure of 5.0×10^{-3} Pa to enhance coating adhesion. The substrate was then sputter-cleaned using argon ion plasma at bias voltages of -500 , -800 , and -1100 V for durations of 2, 3, and 30 min, respectively. TiN layers were deposited using a titanium target with N_2 gas (240 sccm) at a target current of 140 A. The process was conducted in two stages, with bias voltages of -40 and -150 V applied for 10 and 50 min, respectively. Before MoS_2 deposition, the four samples were washed to remove potential surface contaminants, subsequently dried, and stored. The MoS_2 coating was applied using the alcohol droplet technique. $MoSh_2$ powder (60 g/L) was dissolved in 20 mL of alcohol, ultrasonicated for 15 min, and stirred gently for 30 min. The resulting solution was deposited onto the workpiece to form a smooth layer. The samples were placed in an oven and dried at room temperature for two hours. Figure 1 shows the schematic diagram of the entire process for preparing the composite coatings.

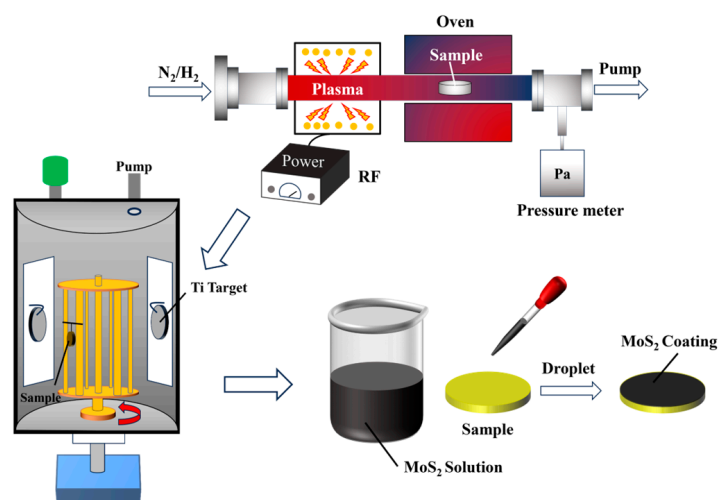


Figure 1. Schematic illustration of the preparation process, including plasma nitriding, multi-arc ion plating deposition of TiN, and MoS_2 coating deposition.

2.2. Structure Characterization

A field-emission scanning electron microscope (FESEM, JSM-7610F, JEOL Ltd., Tokyo, Japan) was used to examine the surface and cross-sectional morphology of the coatings and scratch tracks, as well as to determine their chemical composition. Energy-dispersive X-ray spectroscopy (EDS, NORAN System 7, Thermo Fisher Scientific, Waltham, MA, USA), integrated with the FESEM, was used at an accelerating voltage of 15 kV. The thickness of the TiN coating was measured using EDS. The phase structure of the coating was analyzed by X-ray diffraction (XRD, Smartlab 9, Rigaku, Japan) using Cu-K α radiation, with a scanning step size of 0.05°, scanning rate of 5°/min, and diffraction range of 10–80°. The surface roughness of the coatings was measured using an atomic force microscope (AFM, Dimension 3100, Veeco Instruments Inc., Plainview, NY, USA). Raman spectroscopy (DXR2, Thermo Fisher Scientific, Waltham, MA, USA) equipped with a 532 nm laser was employed to verify the distribution of MoS₂ on the coating surface and wear tracks.

2.3. Mechanical and Tribological Properties

A nanoindentation test (Hystron TriboIndenter, Bruker, Billerica, MA, USA) was conducted to assess the hardness of the samples. Each sample underwent five indentation tests to ensure data reliability. Cross-sectional samples were polished to achieve a mirror finish, after which the cross-sectional hardness of the TC4 substrate and PN was measured using a Vickers hardness tester (FM-700, Future tech, Kawasaki, Japan). Under dry sliding conditions, tribological tests were conducted using a custom ball-and-disk tribometer, with Si₃N₄ balls (6 mm in diameter) as the tribological pair. A normal load of 5 N and a rotational speed of 100 rpm were applied, with a radius of 6 mm and a sliding velocity of 0.063 m·s⁻¹. A scratch tester (MFT-5000, Rtec Instruments, San Jose, CA, USA) was employed to evaluate the adhesion of the TiN coating on the TC4 substrate and PN-2 sample. To evaluate the frictional lifetime of MoS₂ on the surface of different samples, 440C stainless steel balls (6 mm in diameter) were used as the tribological pair. A normal load of 15 N and a rotational speed of 600 rpm were applied, with a radius of 6 mm and a sliding velocity of 0.377 m·s⁻¹. Wear rates were determined using a three-dimensional white light microscope (LSCM, DCM8, Leica, Germany), which measured the depth of the wear tracks, the thickness of the MoS₂ coating, and three-dimensional topography.

3. Results and Discussion

3.1. Plasma Nitriding

Figure 2 illustrates the XRD patterns of the TC4 substrate and the PN samples. TC4 is an (α + β) titanium alloy, with reflections primarily observed from the hexagonal α -Ti phase (PCPDF 00-44-1294) and the body-centered cubic (BCC) β -Ti phase (JCPDS 00-044-1288). The diffraction pattern of the PN sample reveals additional peaks corresponding to tetragonal Ti₂N (JCPDS 00-017-0386) and TiN (JCPDS 00-038-1420), along with the peaks from α -Ti phases. These results confirm that the TC4 substrate was nitrided. According to previous research, the Ti₂N phase dominates after plasma nitriding, while the TiN phase is present in smaller amounts [24,25].

Figure 3 presents the average surface hardness at various loads and the cross-sectional hardness (measured under a 25 g load) of the TC4 substrate and PN samples, as determined using the Vickers microhardness tester. Figure 3a illustrates that the surface hardness of PN samples increases with rising plasma radio frequency (RF) power [26,27]. This trend is primarily due to the higher plasma nitriding power, which enhances nitrogen ion production and their effective dissolution in the substrate. Figure 3b presents the hardness results of the TC4 substrate and PN samples along their cross-sections. TC4 substrate exhibits a uniform hardness of approximately 3.51 (\pm 0.02) GPa across the examined depth

range. In contrast, the nitriding treatment formed nitrided layers with thicknesses of 55 μm (PN-1), 99 μm (PN-2), and 120 μm (PN-3). The hardness of PN-1, PN-2, and PN-3 samples decreases along the base direction after nitriding, eventually approaching the hardness of the TC4 substrate. As the nitriding sputtering power increases, both the nitrided layer thickness and material hardness increase correspondingly [28].

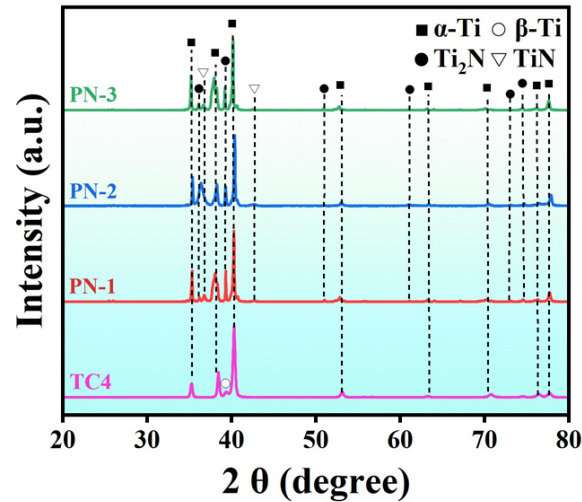


Figure 2. XRD patterns of TC4 substrate and PN samples.

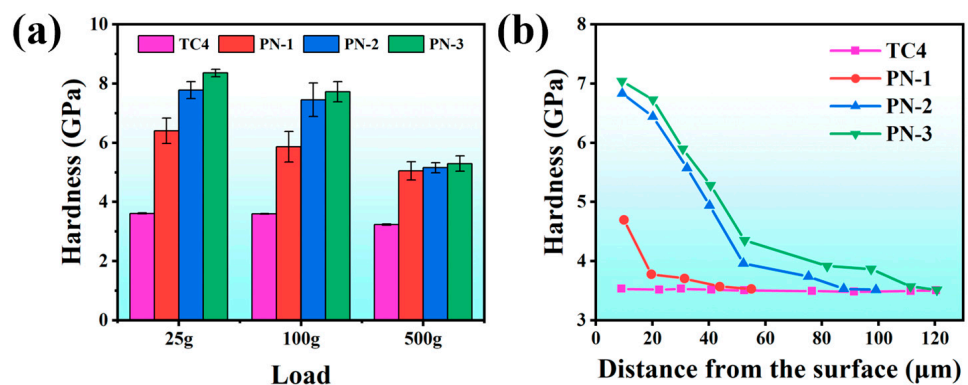


Figure 3. (a) Average surface hardness under different applied normal loads and (b) cross-sectional hardness of the TC4 substrate and PN samples by the Vickers microhardness tester.

Figure 4a presents the results of nanoindentation tests, indicating that the TC4 substrate possesses relatively low hardness and elastic modulus values of 3.9 GPa and 102.6 GPa, respectively. After plasma nitriding, the TC4 substrate showed significant increases in surface hardness and elastic modulus. The PN-3 sample exhibited the most pronounced improvements, with hardness and elastic modulus values of 11.0 GPa and 160.5 GPa, respectively. The PN-2 sample demonstrated the second highest enhancement, with values of 10.9 GPa and 147.3 GPa, while the PN-1 sample showed the least improvement, with values of 9.9 GPa and 140.0 GPa. Notably, the elastic modulus enhancement of the PN-3 sample is particularly remarkable. This enhancement can be attributed to the diffusion of nitrogen atoms during the nitriding process, which may induce microstructural changes within the TC4 substrate, such as grain growth or subcrystalline structures. These changes may also influence the internal stress distribution within the material. Additionally, lattice distortion resulting from ion implantation elevates internal stress [29]. Ultimately, the internal stress generated by heat treatment facilitates the transformation of the β -phase to the α -phase, further contributing to the increase in internal stress. Figure 4c shows the wear rates of the TC4 substrate and PN samples, which were evaluated under dry

friction conditions using a ball-and-disc friction tester. It indicates that the wear rate of the TC4 substrate is markedly higher than that of the PN samples, with a discrepancy of two orders of magnitude, with a wear rate of $1.16 \times 10^{-3} \text{ mm}^3 \cdot \text{N}^{-1} \cdot \text{m}^{-1}$. This is attributable to the lower hardness, elastic modulus and inferior shear resistance of the TC4 substrate, which collectively contribute to a more pronounced wear phenomenon. In contrast, the wear rates of the PN samples were markedly reduced, indicating that the plasma nitriding treatment improved both the hardness and elastic modulus of the PN samples and the load-carrying capacity, and reduced the wear rate. This underscores the importance of enhancing the tribological properties of these materials through the application of surface protection techniques. In particular, the PN-2 sample demonstrated the lowest wear rate of $9.21 \times 10^{-6} \text{ mm}^3 \cdot \text{N}^{-1} \cdot \text{m}^{-1}$, while the wear rates for PN-1 and PN-3 were $12.75 \times 10^{-6} \text{ mm}^3 \cdot \text{N}^{-1} \cdot \text{m}^{-1}$ and $12.62 \times 10^{-6} \text{ mm}^3 \cdot \text{N}^{-1} \cdot \text{m}^{-1}$, respectively. The PN-1 exhibits lower surface hardness and elastic modulus due to less nitrogen ion solid solution, leading to a higher wear rate. In contrast, the PN-3 sample has more nitrogen ion solid solution but lacks a notable hardness increase, and elevated internal stress reduces elastic properties [30]. The mechanical indexes of H/E and H^3/E^2 are crucial for evaluating coating properties, reflecting resistance to elastic and plastic deformation. A higher H/E and H^3/E^2 ratio indicates better wear resistance. [31,32]. This led to reduced H/E and H^3/E^2 ratios, lowering wear resistance. Since PN-2 showed the best performance, subsequent experiments will focus on this sample.

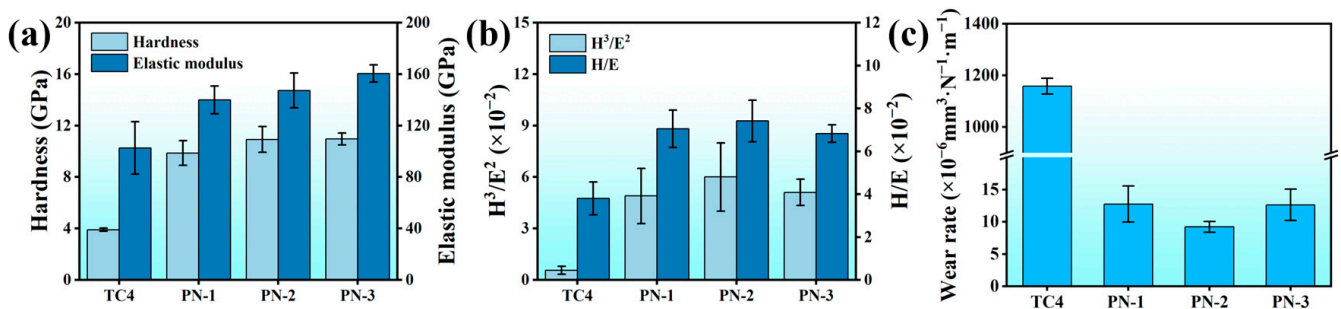


Figure 4. (a) Average nanohardness and elastic modulus, (b) H/E and H^3/E^2 ratio and (c) average wear rates of the TC4 substrate and PN samples.

3.2. Multi-Arc Ion Plating Deposition of TiN

Figure 5 shows the XRD patterns of TC4/TiN and PN-2/TiN, alongside the TC4 substrate and PN-2 sample. The XRD patterns clearly indicate that the TC4/TiN and PN-2/TiN samples exhibit more prominent TiN peaks (JCPDS 00-038-1420). Furthermore, the intensity of the (002) peak corresponding to the TiN coating is more pronounced in comparison to the titanium nitride peak observed in the PN-2 sample.

Figure 6a–d present the surface SEM images of the TC4, PN-2, TC4/TiN and PN-2/TiN samples. The surfaces of the TC4/TiN and PN-2/TiN samples display particles and shallow craters, typical features associated with multi-arc ion plating [33]. Figure 6e–h depict the AFM surface topographies and average surface roughness of the four samples. The surface roughness of all three samples slightly increased. This phenomenon may be attributed to the presence of droplets and pits on the surfaces of the coatings deposited by the multi-arc ion plating process, which contributes to the overall surface roughness [34]. Figure 7 shows the cross-sectional morphology and EDS line scan. The TiN coating exhibits a cross-sectional thickness of 4.85 μm .

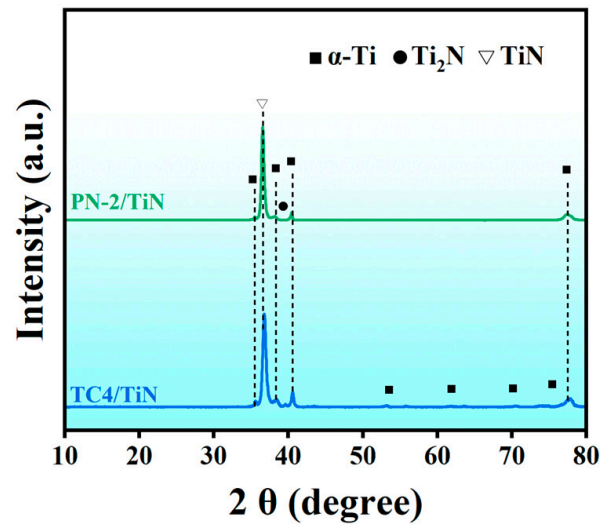


Figure 5. XRD patterns of TC4/TiN and PN-2/TiN.

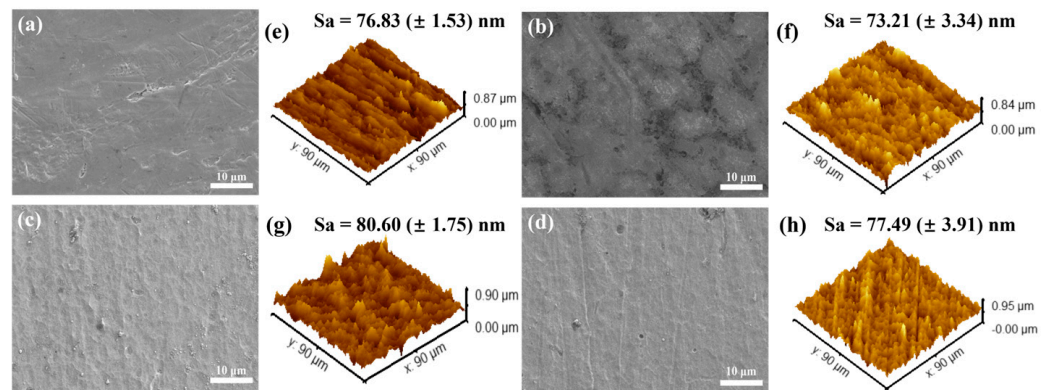


Figure 6. Surface SEM images of the (a) TC4, (b) PN-2, (c) TC4/TiN and (d) PN-2/TiN samples. AFM morphologies and average roughness of the (e) TC4, (f) PN-2, (g) TC4/TiN and (h) PN-2/TiN samples.

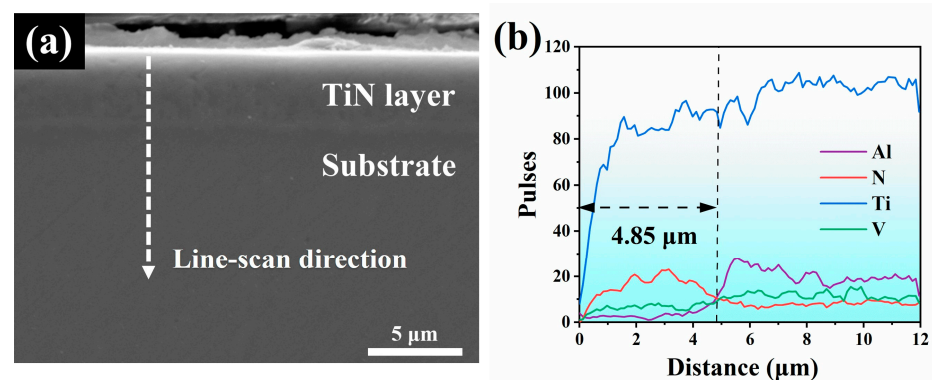


Figure 7. (a) PN-2/TiN cross-sectional morphology of SEM image, (b) EDS line scan.

Figure 8 shows the nanohardness and elastic modulus of the TC4 substrate, PN-2, TC4/TiN and PN-2/TiN samples were characterized through nanoindentation. The results presented in Figure 8a indicate that the hardness of the PN samples is significantly higher compared to the other samples. Comparative analysis reveals that the hardness and elastic modulus of TC4/TiN and PN-2/TiN samples are notably higher than those of the TC4 substrate and PN-2 samples. In particular, samples with an intermediate transition layer, PN-2/TiN, demonstrated improved nanohardness and elastic modulus. Figure 9 shows

the tribological behavior of the four samples which were examined under identical test conditions. Figure 9a shows the COF curves of the four samples. It is evident that the TC4 substrate has obvious friction noise [35] under dry sliding, and the friction coefficient of the PN-2 and PN-2/TiN samples significantly increased. Figure 9b shows the average wear rates of the four samples. In comparison to PN-2/TiN, TC4/TiN exhibited a high wear rate of $1.01 \times 10^{-3} \text{ mm}^3 \cdot \text{N}^{-1} \cdot \text{m}^{-1}$, which is nearly identical to that of the TC4 substrate ($1.16 \times 10^{-3} \text{ mm}^3 \cdot \text{N}^{-1} \cdot \text{m}^{-1}$). The primary reason for this phenomenon is that when the applied load exceeds the yield strength of the TC4 substrate, the substrate undergoes plastic deformation, while the coating, possessing a higher yield strength, remains elastic. This lack of coordinated deformation results in stress concentration [36]. Additionally, due to the differences in elastic modulus, both the substrate and coating experience stress concentration during deformation, particularly at the interface. Concurrently, the discrepancies in mechanical properties may lead to suboptimal bonding between TC4/TiN coatings and PN-2/TiN, potentially resulting in failures such as cracking or peeling. The PN-2/TiN sample exhibited the lowest wear rate of $9.16 \times 10^{-6} \text{ mm}^3 \cdot \text{N}^{-1} \cdot \text{m}^{-1}$.

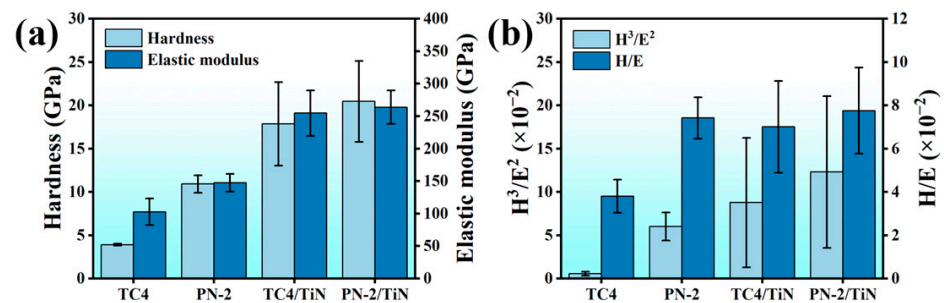


Figure 8. (a) Average nanohardness and elastic modulus, (b) H/E and H^3/E^2 ratio of the TC4 substrate, PN-2, TC4/TiN and PN-2/TiN samples.

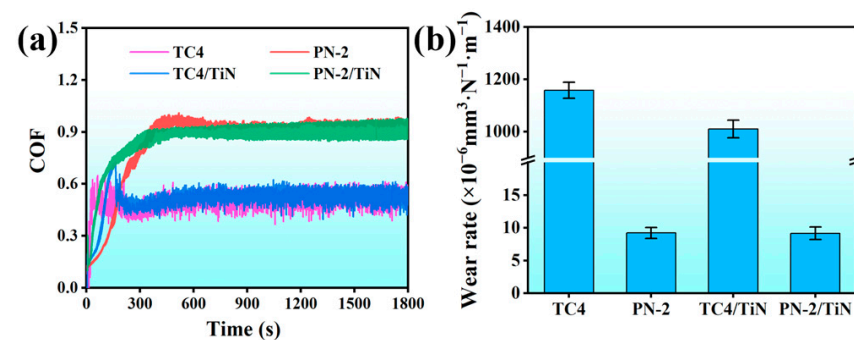


Figure 9. (a) Coefficient of friction under dry friction conditions for 30 min and (b) average wear rates of the TC4 substrate, PN-2, TC4/TiN and PN-2/TiN samples.

In order to investigate the reason for the large difference in wear rate between TC4/TiN and PN-2/TiN, a scratch test was conducted to evaluate the adhesion between the coatings. Figure 10 illustrates the 3D laser scanning confocal microscopies of the scratch tracks of the TC4/TiN and PN-2/TiN samples after the scratch test. The TC4/TiN sample exhibits clear signs of buckling failure at 38 N, resulting in the complete peeling of the TiN coating. Notably, the PN-2/TiN sample exhibited typical buckling failure at a normal load of 58 N, demonstrating superior load-bearing capacity consistent with the nanohardness, H/E, and H^3/E^2 ratio results. In conclusion, the PN-2/TiN sample showed excellent adhesion, with minimal delamination observed at the end of the scratch track, while the TC4/TiN sample exhibited extensive delamination throughout the test. Plasma nitriding is suggested as an effective method to alleviate the inherent incompatibility between the substrate and the protective coating. Figure 11 presents the 3D morphologies of the four samples under dry

friction. Figure 11a reveals severe wear on the TC4 substrate. Figure 11b shows significant wear depth on TC4/TiN, exceeding the TiN coating thickness. The friction coefficient and wear rate further confirm the peeling of the TiN coating. In contrast, the wear tracks of the PN-2 and PN-2/TiN samples are very shallow, consistent with the wear rate results, indicating significantly improved wear resistance.

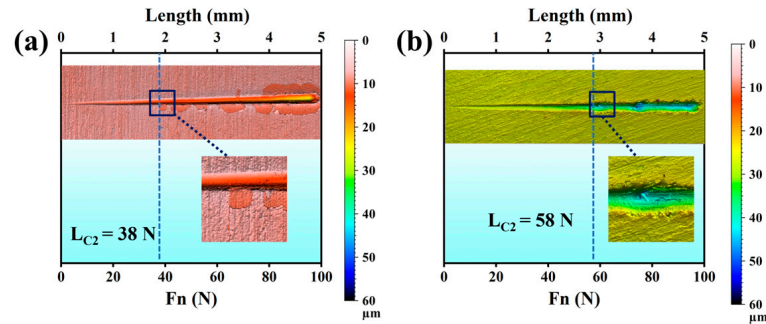


Figure 10. Load and scratch images of the (a) TC4/TiN and (b) PN-2/TiN samples.

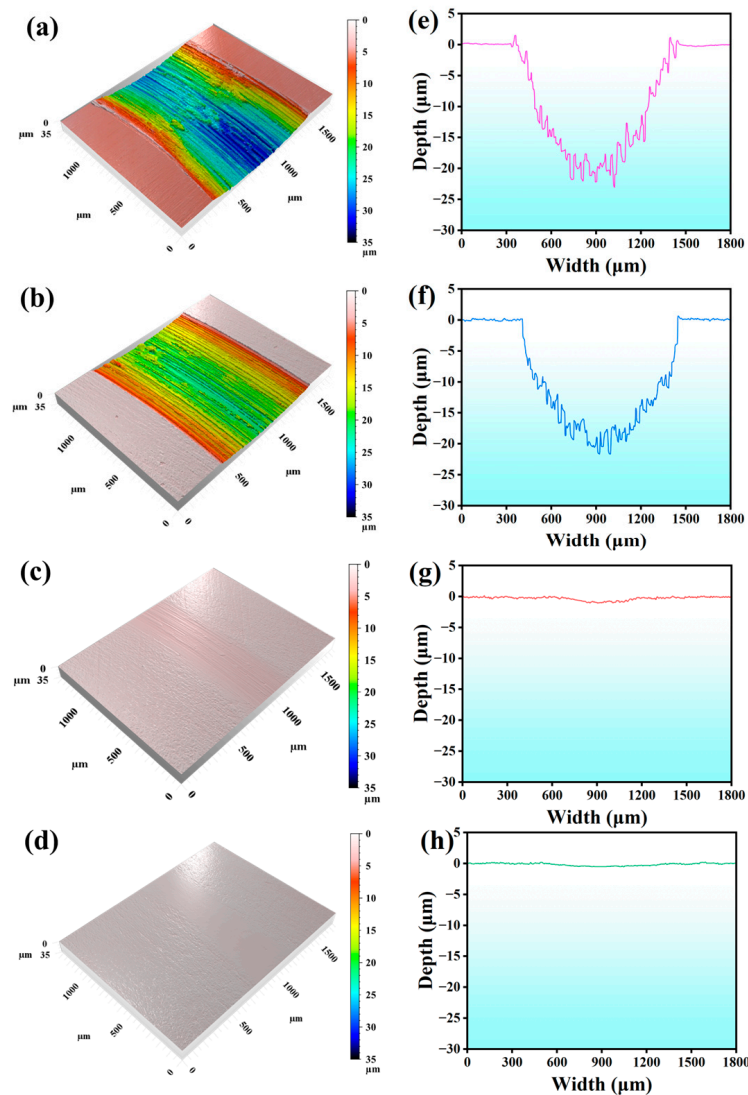


Figure 11. Three-dimensional morphologies of (a) TC4, (b) TC4/TiN, (c) PN-2, and (d) PN-2/TiN and 2D cross-sectional profiles of (e) TC4, (f) TC4/TiN, (g) PN-2, and (h) PN-2/TiN samples after 30 min of friction time.

3.3. MoS₂ Coating Tribological Properties

Figure 12a–c present the SEM images of the MoS₂ coating, showing that the MoS₂ powder is composed of thin flakes with a dense structure. To determine the coating thickness, a mechanical removal process was applied to the coating surface, resulting in a deep groove. The thickness of the MoS₂ coating was then measured using three-dimensional laser scanning confocal microscopy. As shown in Figure 12d,e, the MoS₂ coating has a thickness of approximately 8.83 μm. Figure 12f displays the XRD pattern of the MoS₂ coating, with diffraction peaks corresponding to the 2H-MoS₂ phase (JCPDS 00-037-1492). The prominent (002) peak suggests a layered structure with a specific interlamellar spacing [37].

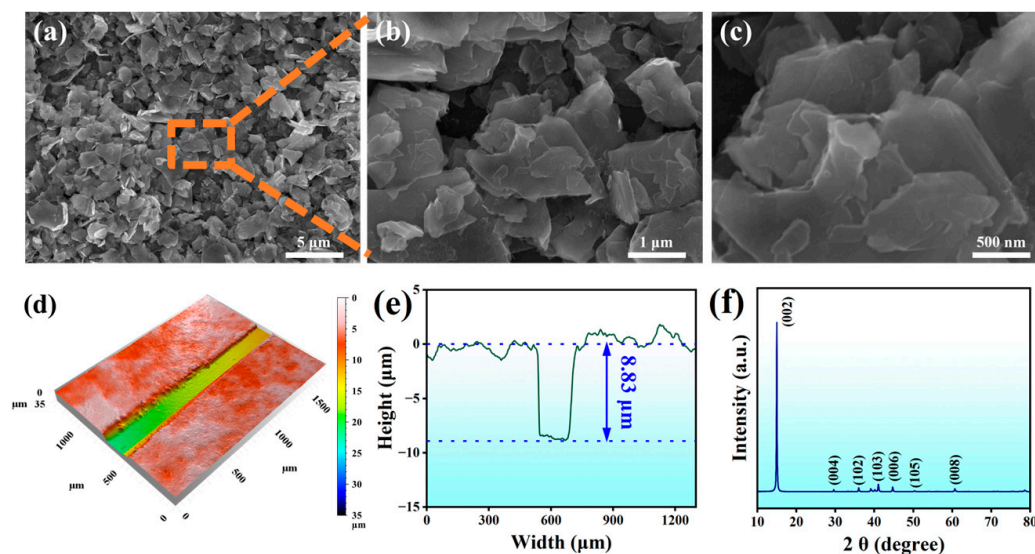


Figure 12. (a–c) SEM images, (d) 3D topography, (e) cross-sectional profile and (f) XRD pattern of the MoS₂ coating.

Figure 13 illustrates the outcomes of friction testing conducted on TC4 substrate, PN-2, TC4/TiN and PN-2/TiN with MoS₂ coating at a relative humidity of 20% ± 2.5%. As shown in Figure 13 the coefficient of friction (COF) for TC4/MoS₂ exhibits a rapid initial increase, reaching a peak value of approximately 0.45. The MoS₂ layer is rapidly removed due to friction. The high friction coefficient and short friction lifetime indicate that the tribological performance of the TC4/MoS₂ sample is insufficient. This is attributed to the low hardness and elastic modulus of the TC4 alloy, which has an extremely limited load-bearing capacity. Consequently, enhancing surface durability is essential to improve the load-bearing capacity. The friction lifetime of MoS₂ coating improved following the surface hardening of the TC4 alloy. As shown in Figure 13, the friction lifetimes of PN-2/MoS₂, TC4/TiN/MoS₂, and PN-2/TiN/MoS₂ samples are 587, 1302 and 1795 s, respectively.

Figure 14 shows the surface morphologies and EDS mapping spectra of the four samples at the 10-min mark of the friction process. Figure 14a depicts the friction condition of TC4/MoS₂, showing exceptionally wide wear tracks and minimal MoS₂ presence. In contrast, the PN-2/MoS₂, TC4/TiN/MoS₂, and PN-2/TiN/MoS₂ samples exhibit narrower wear tracks, indicating higher MoS₂ retention. The wear track of the PN-2/MoS₂ sample shows minimal MoS₂ presence in the wear track, with the edges exhibiting the highest concentration of the material. Additionally, the titanium matrix is entirely exposed in the grinding marks of TC4/MoS₂, whereas the grinding marks of PN-2/MoS₂ also exhibit a distinct nitriding layer. The TC4/TiN/MoS₂ sample displays less exposed substrate, while the PN-2/TiN/MoS₂ sample exhibits minimal TiN layer exposure. To further quantify the MoS₂ accumulation in the wear tracks of the four samples, Raman mappings were obtained

at the 10-min mark of the friction process. The two characteristic peaks of the MoS_2 , namely E^{1}_{2g} peak and A^1_g , correspond to the in-plane vibration of molybdenum and sulfur atoms and the out-of-plane vibration of sulfur atoms, respectively. Figure 15 shows that with increasing surface hardness, the amount of MoS_2 retained in the wear tracks also increases. The combined analysis of EDS mappings and friction coefficient curves confirms that the PN-2/TiN/ MoS_2 sample retains more MoS_2 and exhibits the longest friction lifetime.

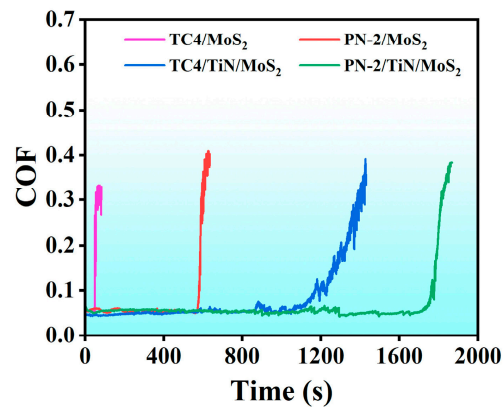


Figure 13. The friction coefficient curves of the TC4/ MoS_2 , PN-2/ MoS_2 , TC4/TiN/ MoS_2 and PN-2/TiN/ MoS_2 samples.

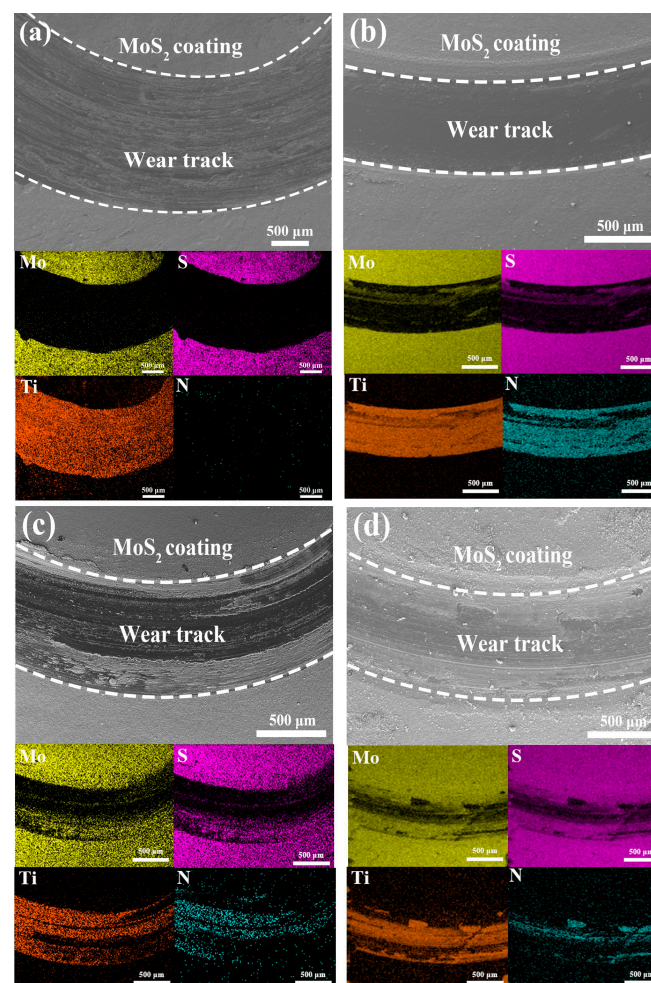


Figure 14. Surface morphologies and EDS mappings of the (a) TC4/ MoS_2 , (b) PN-2/ MoS_2 , (c) TC4/TiN/ MoS_2 and (d) PN-2/TiN/ MoS_2 samples at 10 min of friction time.

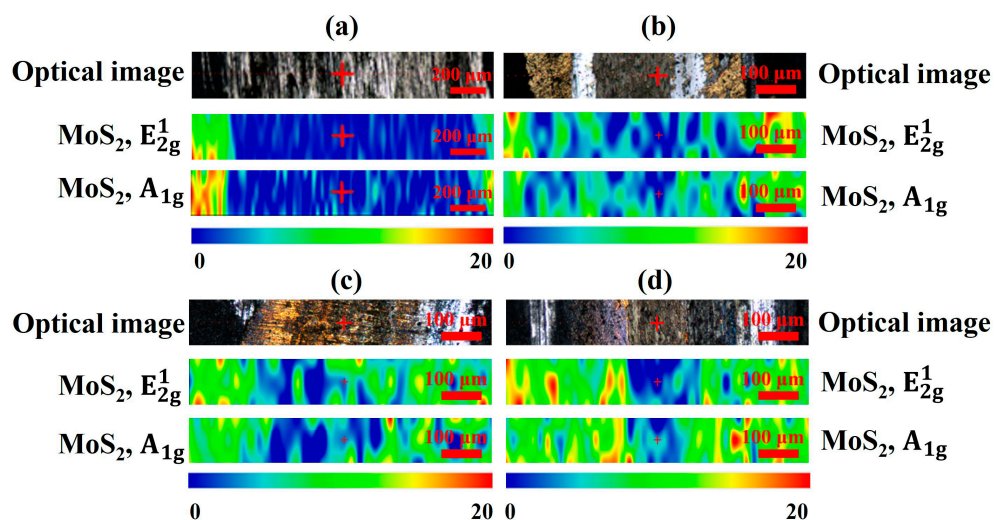


Figure 15. Raman spectra acquired from the wear track of (a) TC4/MoS₂, (b) PN-2/MoS₂, (c) TC4/TiN/MoS₂ and (d) PN-2/TiN/MoS₂ samples at 10 min of friction.

Prior research has indicated that the micro-protrusion architecture present on the surface is capable of accommodating a greater quantity of MoS₂ [37,38]. The friction lifetimes of MoS₂ on different coatings are discussed in further detail in the subsequent section. Figure 16 demonstrates that the matrix significantly affects performance under constant substrate surface roughness and ambient humidity. The friction process can be divided into three phases. In the initial phase, the friction pair directly contacts the MoS₂ layer, functioning as a lubricant. At this stage, the MoS₂ coating remains continuous, ensuring a low friction coefficient. In the second phase, the depletion of the MoS₂ layer leads to contact between the friction pair and the underlying coating, causing fluctuations in the friction coefficient. In the final phase, full depletion of the MoS₂ layer results in direct contact between the friction pair and the coating, significantly increasing the friction coefficient, and resembling dry friction conditions. Under heavy loads, the MoS₂ coating becomes more compact. Microcracks appear on the worn surface due to cyclic friction and plastic deformation. As these microcracks propagate, the coating peels off, forming a transfer film on the counter surface [39]. The quality of this film directly influences the coating's anti-friction properties. Figure 16a clearly shows that TC4 exhibits limited load-bearing capacity due to its insufficient mechanical properties, resulting in the rapid depletion of MoS₂. Conversely, Figure 16b shows improved surface hardness in PN-2, enhancing its load-bearing capacity. Figure 16c further illustrates that the surface hardness of TC4/TiN is even greater, thereby providing enhanced protective performance. However, following the initial contact phase, the MoS₂ and TiN coating display inadequate resistance to plastic deformation. This issue is exacerbated by weak interfacial adhesion between the coating and substrate, leading to friction coefficient fluctuations and eventual delamination. In contrast, the PN-2/TiN coating shows the highest hardness, optimal adhesion between PN-2 and TiN, and the longest operational life of the MoS₂ coating under frictional conditions.

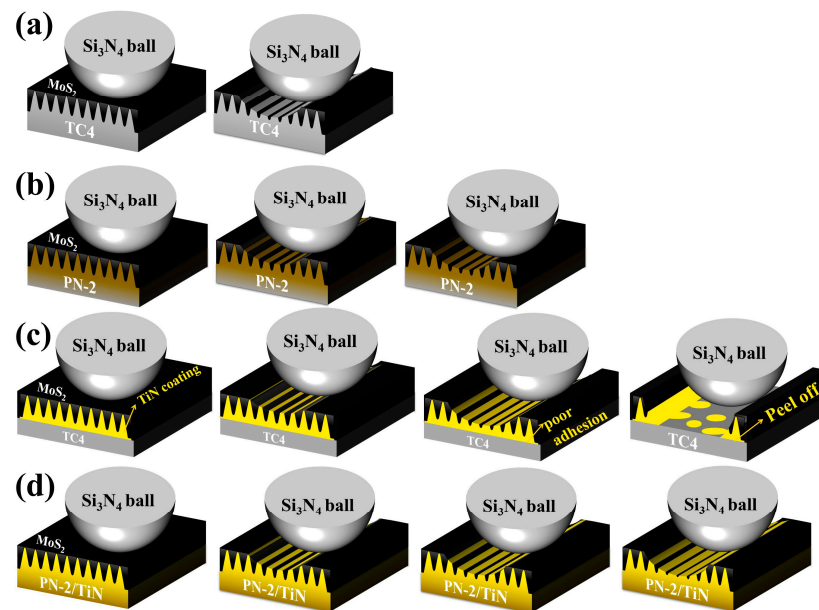


Figure 16. Schematic of the wear mechanism of (a) TC4/MoS₂, (b) PN-2/MoS₂, (c) TC4/TiN/MoS₂ and (d) PN-2/TiN/MoS₂.

4. Conclusions

In summary, this research presents plasma nitriding and multi-arc ion plating combined treatments for enhancing the mechanical performance of the TC4 alloy, and the key findings of this study can be summarized as follows:

- The combined treatment coatings were deposited on TC4 alloy using plasma nitriding and multi-arc ion plating to improve wear resistance.
- Plasma nitriding treatment enhances the adhesion performance between the TC4 substrate and TiN coating.
- The primary factor influencing the friction lifetime of MoS₂ is surface hardness; specifically, an increase in surface hardness correlates with an extended friction lifetime. This phenomenon is attributed to the material robust load-bearing capability.
- The PN-2/TiN/MoS₂ coating offers a promising approach to enhance the tribological properties of TC4 alloys, ultimately contributing to the development of improved tribological systems.

Author Contributions: Conceptualization and methodology, K.L., L.Z., Z.Y. and S.X.; formal analysis and investigation, K.L., Z.Y. and S.X.; validation, H.L.; writing—original draft preparation, H.L.; writing—review and editing, K.L., G.W., Z.R., L.Z., Z.Y., Z.R., Y.L. and S.X.; All authors have read and agreed to the published version of the manuscript.

Funding: This research was funded by the Strategic Priority Research Program of the Chinese Academy of Sciences (Grant No. XDB0470102), the fund of the Excellent Youth Science Foundation of Shandong Province (Grant No. 2022HWYQ-096), the fund of Natural Science Foundation of Shandong Province (Grant No. ZR2022QE162, ZR2024QA223, ZR2024QE526), the Key Research and Development Program in Shandong Province (No. SYS202203), the Key Research Project of Shandong Provincial Natural Science Foundation (No. ZR2023ZD13), the Scientific Instrument Development Program of the Chinese Academy of Sciences (No. PTYQ2024YZ0006), the Key Instrument Development Program of the National Natural Science Foundation of China (No. 52427807), the Key Research Project of Shandong Provincial Natural Science Foundation (No. 2024KJHZ017), and the Program for Taishan Scholars of Shandong Province.

Data Availability Statement: Data is contained within the article.

Acknowledgments: The authors sincerely acknowledge Shusheng Xu for his interest and help in relation to the work, which made it possible to continue this study.

Conflicts of Interest: Hongyu Li, Ganggang Wang, Zhenghao Ren, and Liwei Zheng are employed by the Shandong Laboratory of Advanced Materials and Green Manufacturing at Yantai. Kai Le is employed by Yantai Zhongke Research Institute of Advanced Materials and Green Chemical Engineering. The remaining authors declare that the research was conducted in the absence of any commercial or financial relationships that could be construed as a potential conflict of interest.

References

1. Sarraf, M.; Rezvani Ghomi, E.; Alipour, S.; Ramakrishna, S.; Liana Sukiman, N. A State-of-the-Art Review of the Fabrication and Characteristics of Titanium and Its Alloys for Biomedical Applications. *Biores Manuf.* **2022**, *5*, 371–395. [[CrossRef](#)] [[PubMed](#)]
2. Sun, K.; Dong, Y.; Yao, L.; Mahapatra, M.; Xu, Y. Surface Lubrication with Thermal- and PH-Sensitive PNIPAM-Co-PAA-(IF-MoS₂/GO) Composite Microgels under YG8/TC4 Contact. *Appl. Surf. Sci.* **2024**, *669*, 160461. [[CrossRef](#)]
3. Yetim, A.F.; Yildiz, F.; Vangolu, Y.; Alasaran, A.; Celik, A. Several Plasma Diffusion Processes for Improving Wear Properties of Ti6Al4V Alloy. *Wear* **2009**, *267*, 2179–2185. [[CrossRef](#)]
4. Wang, J.; Lu, H.; Wen, Z.; Lian, Y.; Li, Z.; Yue, Z. Prediction of Fatigue Life of TC4 Titanium Alloy Based on Normalized Equivalent Initial Flaw Size Model. *Theor. Appl. Fract. Mec.* **2022**, *122*, 103563. [[CrossRef](#)]
5. Zhao, Y.; Lu, M.; Fan, Z.; Huang, S.; Huang, H. Laser Deposition of Wear-Resistant Titanium Oxynitride/Titanium Composite Coatings on Ti-6Al-4V Alloy. *Appl. Surf. Sci.* **2020**, *531*, 147212. [[CrossRef](#)]
6. Kuang, F.; Pan, Y.; Sun, J.; Liu, Y.; Lei, C.; Lu, X. Crafting High-Strength and Ductile Powder Metallurgy Ti6Al4V Alloy with a Multi-Scale Microstructure. *Mater. Sci. Eng. A* **2024**, *892*, 146054. [[CrossRef](#)]
7. Guo, Y.; Lu, X.; Han, W.; Min, J.; Dai, G.; Sun, Z.; Chang, H.; Xia, Y. Effect of WC Addition on Microstructure and Properties of Laser Melting Deposited Ti6Al4V. *Mater. Charact.* **2024**, *217*, 114344. [[CrossRef](#)]
8. Huang, L.; Yuan, J.; Li, C. Influence of Titanium Concentration on Mechanical Properties and Wear Resistance to Ti6Al4V of Ti-C:H on Cemented Carbide. *Vacuum* **2017**, *138*, 1–7. [[CrossRef](#)]
9. Wang, L.; Cai, X.; Shi, B.; Zhang, J.; Zhan, X. Direct Energy Deposition of TiC/Ti6Al4V Graded Materials and Heat Resistance Improvement during the Ablation Process. *J. Mater. Res. Technol.* **2024**, *33*, 8482–8490. [[CrossRef](#)]
10. Shi, B.; Huang, S.; Zhu, P.; Xu, C.; Guo, P.; Fu, Y. In-Situ TiN Reinforced Composite Coatings Prepared by Plasma Spray Welding on Ti6Al4V. *Mater. Lett.* **2020**, *276*, 128093. [[CrossRef](#)]
11. Luo, Y.J.; Chen, J.B.; Wang, X.F.; Zhao, Y.X.; Zhang, A.B.; Xie, C.; Chen, Y.; Du, J.K. A Micromechanical Model to Study the Closure Stress Effect on Fatigue Life of Ti6Al4V Subjected to Laser Shock Peening. *Eng. Fract. Mech.* **2018**, *200*, 327–338. [[CrossRef](#)]
12. Li, H.; Sun, Y.; Zhang, J. Effect of ZrO₂ Particle on the Performance of Micro-Arc Oxidation Coatings on Ti6Al4V. *Appl. Surf. Sci.* **2015**, *342*, 183–190. [[CrossRef](#)]
13. Ceschini, L.; Lanzoni, E.; Martini, C.; Prandstraller, D.; Sambogna, G. Comparison of Dry Sliding Friction and Wear of Ti6Al4V Alloy Treated by Plasma Electrolytic Oxidation and PVD Coating. *Wear* **2008**, *264*, 86–95. [[CrossRef](#)]
14. Strakowska, P.; Beutner, R.; Gnyba, M.; Zielinski, A.; Scharnweber, D. Electrochemically Assisted Deposition of Hydroxyapatite on Ti6Al4V Substrates Covered by CVD Diamond Films—Coating Characterization and First Cell Biological Results. *Mater. Sci. Eng. C* **2016**, *59*, 624–635. [[CrossRef](#)]
15. Lima, G.D.; Nascimento, B.L.; de Souza Alves Júnior, I.; Trindade, M.P.; Griza, S. Fatigue Behavior and Life Predictions of Thermally Oxidized Ti6Al4V Alloy According to Oxidation Parameters. *Eng. Fail. Anal.* **2021**, *130*, 105737. [[CrossRef](#)]
16. Vorobyova, M.; Biffoli, F.; Giurlani, W.; Martinuzzi, S.M.; Linser, M.; Caneschi, A.; Innocenti, M. PVD for Decorative Applications: A Review. *Materials* **2023**, *16*, 4919. [[CrossRef](#)]
17. Kamat, A.M.; Copley, S.M.; Todd, J.A. A Two-Step Laser-Sustained Plasma Nitriding Process for Deep-Case Hardening of Commercially Pure Titanium. *Surf. Coat. Technol.* **2017**, *313*, 82–95. [[CrossRef](#)]
18. Sun, F.; Liu, X.L.; Luo, S.Q.; Xiang, D.D.; Ba, D.C.; Lin, Z.; Song, G.Q. Duplex Treatment of Arc Plasma Nitriding and PVD TiN Coating Applied to Dental Implant Screws. *Surf. Coat. Technol.* **2022**, *439*, 128449. [[CrossRef](#)]
19. Yang, J.; Le, K.; Chen, H.; Zhao, X.; Xie, X.; Luo, Y.; Xu, S.; Liu, W. The Significantly Enhanced Mechanical and Tribological Performances of the Dual Plasma Nitrided and PVD Coated Ti6Al4V Alloy. *Int. J. Precis. Eng. Man.* **2023**, *24*, 607–619. [[CrossRef](#)]
20. Hu, Y.; Wang, J.; Li, W.; Tang, X.; Tan, T.; Li, Z.; Feng, H.; Zhang, G. The Effects of Ti Content on Tribological and Corrosion Performances of MoS₂-Ti Composite Films. *Vacuum* **2024**, *221*, 112889. [[CrossRef](#)]
21. Wang, X.; Ma, C.; Yang, G.; Zhang, S.; Zhang, Y.; Jiang, Z.; Yu, L.; Zhang, P. Preparation of Molybdenum Disulfide/Bentonite Nanohybrid and Its Tribological Properties as Lubricant for Water-Based Drilling Fluids. *Tribol. Int.* **2025**, *202*, 110309. [[CrossRef](#)]
22. Liu, X.; Le, K.; Yang, W.; Liu, Y.; Luo, Y.; Zheng, X.; Chen, H.; Xu, S.; Liu, W. Tailoring the Crystallinity and Phase Composition of MoS₂ Nanosheets for Better Lubrication Performance. *Appl. Surf. Sci.* **2024**, *673*, 160856. [[CrossRef](#)]

23. Liang, J.; Le, K.; Liu, Y.; Jang, Y.J.; Jiang, F.; Yang, Z.; Li, H.; Xu, S.; Liu, W. Adaptive Tribological Performance of Porous TiCN-MoS₂ Composite Coatings in Response to Fluctuating Humidity Conditions. *Surf. Coat. Technol.* **2024**, *482*, 130666. [[CrossRef](#)]
24. Zhang, J.; Li, K.; Hu, J. Performances Investigation of Ti6Al4V Alloy Modified by Plasma Nitriding + Plasma Enhanced Chemical Vapor Deposition and Laser Remelting Process in Simulated Body Fluid. *Met. Mater. Int.* **2021**, *27*, 4757–4767. [[CrossRef](#)]
25. Yumusak, G.; Leyland, A.; Matthews, A. The Effect of Pre-Deposited Titanium-Based PVD Metallic Thin Films on the Nitrogen Diffusion Efficiency and Wear Behaviour of Nitrided Ti Alloys. *Surf. Coat. Technol.* **2020**, *394*, 125545. [[CrossRef](#)]
26. El-Hossary, F.M.; Negm, N.Z.; Khalil, S.M.; Raaif, M. Surface Modification of Titanium by Radio Frequency Plasma Nitriding. *Thin Solid. Films* **2006**, *497*, 196–202. [[CrossRef](#)]
27. Li, M.; Xu, X.; Wu, W.; Peng, S.; Chen, W.; Zhai, Z.; Luo, Q.; Peng, H.; Zhang, A. Development and Diagnostic Study of the RF Nitrogen Atom Source. *Vacuum* **2025**, *231*, 113820. [[CrossRef](#)]
28. Ata, M.H.; El-Lateef, H.M.A.; Elrouby, M. Effects of Plasma Powers on the Corrosion, Mechanical, Wear, and Tribological Surface Features of the Fe₅₂Ni₂₈Co₁₇Ti₃ Shape Memory Alloy. *Sur. Interfaces* **2021**, *26*, 101384. [[CrossRef](#)]
29. Galdikas, A.; Petraitiene, A.; Moskaliuviene, T. Internal Stress Assisted Nitrogen Diffusion in Plasma Nitrided Medical CoCr Alloys. *Vacuum* **2015**, *119*, 233–238. [[CrossRef](#)]
30. Daymond, M.R. Internal Stresses in Deformed Crystalline Aggregates. *Rev. Mineral Geochem.* **2006**, *63*, 427–458. [[CrossRef](#)]
31. Li, L.; Lu, Z.; Pu, J.; Hou, B. Investigating the Tribological and Corrosive Properties of MoS₂/Zr Coatings with the Continuous Evolution of Structure for High-Humidity Application. *Appl. Surf. Sci.* **2021**, *541*, 148453. [[CrossRef](#)]
32. Zheng, J.; Hao, J.; Liu, X.; Gong, Q.; Liu, W. TiN/TiCN Multilayer Films Modified by Argon Plasma Treatment. *Appl. Surf. Sci.* **2013**, *280*, 764–771. [[CrossRef](#)]
33. Yang, Z.; Shi, X.; Wu, C.; Zhou, H.; Guo, M.; Liu, S.; Lin, J.; Fu, C. Study on Tribological and Friction Noise Performance of Ti6Al4V Self-Lubricating Composites. *J. Mater. Eng. Perform.* **2019**, *28*, 6063–6072. [[CrossRef](#)]
34. Chen, Q.; Wu, G.; Li, D.; Li, A.; Shang, L.; Lu, Z.; Zhang, G.; Wu, Z.; Tian, G. Understanding the Unusual Friction Behavior of TiN Films in Vacuum. *Tribol. Int.* **2019**, *137*, 379–386. [[CrossRef](#)]
35. Zhou, H.; Shi, X.; Yang, Z.; Wu, C.; Lu, G.; Xue, Y.W. Tribological Property and Frictional Noise Performance of Titanium Alloys with Sn–Ag–Cu and TiC Filled into Surface Dimples. *Tribol. Int.* **2020**, *144*, 106121. [[CrossRef](#)]
36. Zhao, H.; Liu, Z.; Yu, C.; Liu, C.; Zhan, Y. Finite Element Analysis for Residual Stress of TC4/Inconel718 Functionally Gradient Materials Produced by Laser Additive Manufacturing. *Opt. Laser Technol.* **2022**, *152*, 108146. [[CrossRef](#)]
37. Chen, H.; Wang, W.; Le, K.; Liu, Y.; Gao, X.; Luo, Y.; Zhao, X.; Liu, X.; Xu, S.; Liu, W. Effects of Substrate Roughness on the Tribological Properties of Duplex Plasma Nitrided and MoS₂ Coated Ti6Al4V Alloy. *Tribol. Int.* **2024**, *191*, 109123. [[CrossRef](#)]
38. Wang, C.; Zhang, J.; Le, K.; Niu, Y.; Gao, X.; Che, Q.; Xu, S.; Liu, Y.; Liu, W. Effect of Substrate Roughness and Contact Scale on the Tribological Performance of MoS₂ Coatings. *Lubricants* **2023**, *11*, 191. [[CrossRef](#)]
39. Kong, N.; Wei, B.; Li, D.; Zhuang, Y.; Sun, G.; Wang, B. A Study on the Tribological Property of MoS₂/Ti-MoS₂/Si Multilayer Nanocomposite Coating Deposited by Magnetron Sputtering. *RSC Adv.* **2020**, *10*, 9633–9642. [[CrossRef](#)]

Disclaimer/Publisher’s Note: The statements, opinions and data contained in all publications are solely those of the individual author(s) and contributor(s) and not of MDPI and/or the editor(s). MDPI and/or the editor(s) disclaim responsibility for any injury to people or property resulting from any ideas, methods, instructions or products referred to in the content.